



HAL
open science

Exploring the short and long-range order in connection with fluorine content in mixed anions copper hydroxyfluorides

Helies Hyrondelle, Matthew R. Suchomel, Vincent Rodriguez, Alexandre Fargues, Étienne Durand, François Weill, Alain Demourgues

► **To cite this version:**

Helies Hyrondelle, Matthew R. Suchomel, Vincent Rodriguez, Alexandre Fargues, Étienne Durand, et al. Exploring the short and long-range order in connection with fluorine content in mixed anions copper hydroxyfluorides. *Solid State Sciences*, 2024, 147, pp.107384. 10.1016/j.solidstatesciences.2023.107384 . hal-04331803

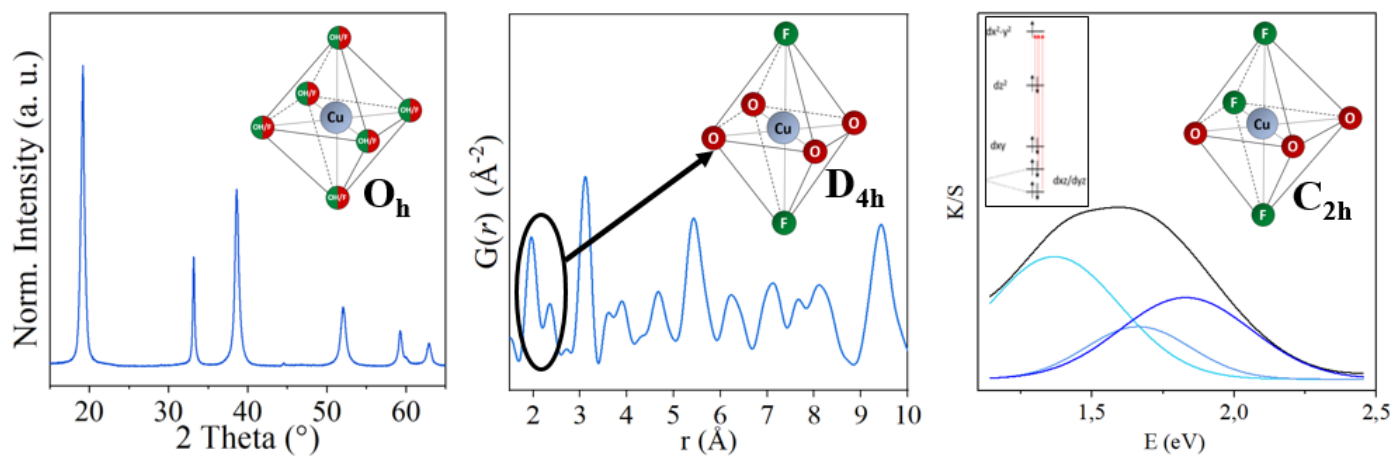
HAL Id: hal-04331803

<https://hal.science/hal-04331803>

Submitted on 13 Dec 2023

HAL is a multi-disciplinary open access archive for the deposit and dissemination of scientific research documents, whether they are published or not. The documents may come from teaching and research institutions in France or abroad, or from public or private research centers.

L'archive ouverte pluridisciplinaire **HAL**, est destinée au dépôt et à la diffusion de documents scientifiques de niveau recherche, publiés ou non, émanant des établissements d'enseignement et de recherche français ou étrangers, des laboratoires publics ou privés.



Exploring the anionic order and octahedron symmetry

Exploring the short and long-range order in connection with fluorine content in mixed anions copper hydroxyfluorides

Helies Hyondelle^{1,*}, Matthew R. Suchomel¹, Vincent Rodriguez², Alexandre Fargues¹, Etienne Durand¹, François Weill¹, and Alain Demourgues^{1,*}

*Corresponding authors : helies.boumali@icmcb.cnrs.fr , alain.demourgues@icmcb.cnrs.fr

¹CNRS, University of Bordeaux, Bordeaux INP, ICMCB UMR CNRS 5026, F-33600 Pessac, France

²Institut des Sciences Moléculaires, UMR 5255 CNRS, University of Bordeaux, F-33405 Talence Cedex, France

Abstract

Hydroxyl-rich (Cu-LF) and Fluorine-rich (Cu-HF) copper hydroxyfluorides $\text{Cu}(\text{OH})_{2-x}\text{F}_x$ ($x=0.4-0.5$ and $x=0.9-1.5$) were prepared by precipitation route followed by hydrothermal process where the starting pH and the HF molar content play a key role. Based on powder XRD and PDF analysis, long range and short order were evidenced with various Cu-O/F bondlengths illustrating the Jahn-teller distortion as well as the Cu-Cu intra-sheet and interslab interactions. Tuning the fluorine content allows chemical bonding modulation by antagonist effect, resulting for instance in the weakening of H bonding in the hydroxyl-rich compound. When the fluorine content increases, the average structures evolve from a disordered network with a random distribution of anions in the vicinity of Cu^{2+} in Cu-LF to a well ordered mixed anions phase where $\text{Cu}(\text{OH})_3\text{F}_3/\text{Cu}(\text{OH})_2\text{F}_4/\text{Cu}(\text{OH})_5\text{F}$ distorted octahedra are close to C_{2h} point group symmetry. Raman spectroscopy confirm the average structural features with the point group symmetry. One should outline in Cu-HF composition, stronger $\text{CuF}_3(\text{OH})_3$ octahedron stiffness associated to a stretching O-H mode at lower frequency, synonymous of O-H bond weakening and consequently stronger hydrogen bonding in agreement with PDF analysis. UV-visible-NIR spectra show in Cu-HF hydroxyfluoride, an increase of the optical band gap of 0.6 eV and a decrease of $\text{Cu}^{2+}(3d^9)$ crystal field splitting of 0.1 eV in agreement with the larger fluorine content. However, the $d_{xz}-d_{yz}$ orbital splitting increases of 0.2 eV in Cu-HF in good agreement with the C_{2h} point group symmetry and the related distortion. Finally, whereas the hydroxyl-rich Cu-LF phase decomposes into CuO at $T>300^\circ\text{C}$, the Fluorine rich Cu-HF compound lead at $T>320^\circ\text{C}$ to the formation of CuF_2 , Cu_2O in addition to CuO. This unusual reduction process $\text{Cu}^{2+} \rightarrow \text{Cu}^+$ at low temperature is associated to the strengthening of Cu-O/F and Cu-Cu bonding in the basal plane of $\text{Cu}(\text{OH})_3\text{F}_3$ distorted octahedron.

1. Introduction

Transition metal hydroxides represent a unique class of materials and are commonly used as cathodes for alkaline batteries¹, supercapacitors^{2,3}, inorganic pigments⁴, and electrochromic devices⁵ as well as catalysts and electrocatalysts⁶ for oxygen evolution reaction. In these 2D structures, it is crucial to understand what occurs within the interslab space. For instance, in nickel hydroxides structures, depending on the strength of weak interactions (hydrogen bondings and Van der Waals interactions) and the water molecules between the slabs, the structure can exhibit disorder, stacking faults and interstratification phenomena^{7,8}. These structural modifications are giving rise to different polymorphs α/β -Ni(OH)₂ with different properties. The common way to tune the hydrogen bonding is to modify the cation nature, but this is also possible to focus on the anions, giving rise to “mixed-anions” structures.

Mixed-anions compounds offers a tremendous diversity, as it can induce unusual coordinations correlated to modulate properties through the anionic solid solution⁹. Historically, oxyfluorides materials have been widely studied, mostly for optical applications¹⁰. Stabilizing compounds with anions of different valence, electronegativity or ionic size is a true challenge, but it seems to be easier in hydroxyfluorides (HyF) where the effective ionic radii of F⁻ and OH⁻ are relatively close but the χ_{OH} electronegativity can vary depending on the strength of hydrogen bonding. Moreover, most of 3d transition metal oxides are considered a base and in particular copper oxide CuO. Most of divalent metals and transition metal HyF M(OH)F (M = Mg, Fe, Co, Zn) crystallize with an orthorhombic unit cell (Pnma) with infinite planes along (010) of edge sharing M(OH)₃F₃ octahedra pairs linked by bridging OH sites and by corner sharing at F sites¹¹⁻¹⁴. Then, in this 3D framework related to diaspre-AIOOH, strong hydrogen bonding acts into the 3D tunnels around the distorted octahedral site with D_{2h} point group symmetry, formed by mixed anions O/F. Other structural types can be obtained by cation substitution, such as Mn(OH)F and Cd(OH)F crystallizing with a distorted rutile-type structure (CaCl₂-type)^{14,15}. Two copper HyF structures have already been synthesized in literature¹⁶ by hydrothermal synthesis at temperatures between 100 and 230°C. The structures obtained were characterized by single crystal X-ray diffraction analysis and are more or less related to brucite-like network. The first one is CuOHF (P2₁/a), a layer structure where the edge-sharing distorted octahedra form buckled sheets. The second one, Cu₃(OH)₂F₄ (or Cu(OH)_{0.66}F_{1.33}) (P2₁/n) with an higher F/OH ratio becomes more tridimensional and remind the diaspre 3D-channel framework previously described. The Jahn-Teller distortion is very recognizable in these compounds, leading to CuF₄(OH)₂ distorted octahedron with 4 Cu-O/F shorter bondlengths between 1.91 Å and 1.98 Å and 2 longer ones between 2.30 and 2.34 Å. These values are similar in the distorted rutile structure of CuF₂ with 4 Cu-F at 1.92 Å and 2 longer ones at 2.30 Å¹⁷. An almost identical polyhedra is noticed for Cu(OH)F layer

structure. The local environment of Cu^{2+} strongly changes with pure hydroxide $\text{Cu}(\text{OH})_2$ where Cu^{2+} ions are now stabilized in a square pyramid¹⁸. This hydroxide crystallizes with an orthorhombic symmetry ($Cmc2_1$) by revealing zig-zag chains of edge-sharing octahedra and a lower 2D character, showing the key role of hydrogen bonding in association with the Jahn-Teller effect of Cu^{2+} .

Hydroxyl-rich copper hydroxyfluorides $\text{Cu}(\text{OH})_{1+x}\text{F}_{1-x}$ have never been explored. Then, we tried to synthesize it by using softer routes such as co-precipitation and low temperature hydrothermal synthesis. Modulating the OH/F molar ratio could lead to the tunability of Cu-O/F bonds, affecting the Cu^{2+} crystal field and thermal decomposition or still the reactivity. This work dealt with the synthesis and characterization of two compositions OH-rich and F-rich and the characterization of long-range and short-range order by powder X-Ray analysis (XRD and PDF) and Raman spectroscopy. UV-Visible-NIR spectroscopy allows determining the evolution of optical band gap and Cu^{2+} d-d electronic transitions highlighting the Jahn-Teller distortion. Finally, the TGA measurement under argon will give information about the thermal stability of Cu hydroxyfluorides and of the Cu^{2+} local environments.

2. Experimental section

2.1. Characterization

2.1.1 X-Ray diffraction

Long range average structure of copper hydroxyfluorides structures were identified using powder X-ray diffraction pattern collected with Bragg-Brentano geometry PANalytical X'Pert MPD Pro diffractometer with a $\text{Cu K}\alpha$ source ($\lambda = 1.5418 \text{ \AA}$) at room temperature. The step size is 0.02° with a step time of 1.2s. The acquisition was performed at 40kV and 40mA in the 2θ range from 8 to 80° . The JANA2006¹⁹ program was used for pattern matching and structural refinement.

2.1.1 Pair distribution function experiments

Short range structural order was examined by Pair Distribution Function (PDF) analysis. Powders were measured with a capillary Debye-Scherrer geometry Bruker D8 diffractometer with a Mo source ($\lambda=0.71 \text{ \AA}$) and DECTRIS EIGER2 500K detector. A variable collection time strategy optimizing high angle and counting statistics allowed a total scattering data up to $Q_{\text{max}} \sim 17 \text{ \AA}^{-1}$. Powders were loaded in 0.3mm diameter borosilicate capillaries. A background pattern was obtained using the same empty capillaries. The total scattering data measured was converted to a reduced pair distribution function $G(r)$ using the PDFgetX3 software package²⁰. Theoretical PDF $G(r)$ curves for complete and partial in the copper hydroxyfluorides nanostructures were simulated using PDFgui²¹

2.1.2 Raman spectroscopy analysis

Raman spectra were recorded at room temperature on a HR800 confocal Raman microscope from Horiba Scientific (Olympus MPLAN objective 100×, NA=0.90), using a CW 532 nm laser excitation. The spectrometer included a grating with 1800 grooves/mm and a nitrogen cooled CCD camera at 140K. The laser power was lower than 1mW to avoid sample damage (blue powder). Unpolarised Raman spectra were measured in the low frequency range 200–600 cm⁻¹ with acquisition times of 300 s averaged 3 times and in the high frequency range 3000-4000 cm⁻¹ with acquisition times of 30 s averaged 3 times. In both case the confocal/spatial hole of 100 μm gave a spectral resolution better than 2 cm⁻¹.

2.1.2 Optical analysis

Optical absorption spectra were recorded between 200 and 2000 nm with a step of 1 nm and a band length of 2 nm on a Cary 5000 (Varian) spectrophotometer using an integration sphere. The rough data were transformed using the Kubelka-Munk function: $K/S = (1-R)^2/2R$ with K, S and R respectively the coefficients of absorption, scattering and diffuse reflection.

2.2. Copper hydroxyfluorides synthesis and characterization

Cu(OH)_{2-x}F_x powders were prepared from copper acetate monohydrate (Cu(CO₂CH₃)₂·H₂O 99%, Aldrich), hydrofluoric acid (HF 40%, VWR) and aqueous ammonium hydroxide (NH₄OH 35%, Fischer). Two different compositions were targeted: a low fluorine Cu(OH)_{2-x}F_x pure phase (Cu-LF) is obtained for very short co-precipitation (CP) time at room temperature. A more fluorinated phase is also stable but requires higher temperature and synthesis duration; the latter conditions are carried out by microwave assisted hydrothermal synthesis (MW), using CEM MARS apparatus.

2.2.1. Low Fluorine (Cu-LF) Phase

An aqueous solution of aqueous copper acetate was prepared in De-Ionized (DI) water (0.125M, 80mL) where hydrofluoric acid was added (F/M ratio = 1). Ammonium hydroxide was added dropwise (OH/M ratio = 1) under stirring to form a blue precipitate. After 5 minutes of reaction 25°C, the blue precipitate was collected by centrifugation, washed several times with DI water and dried in an oven for 6 hours at 80°C.

2.2.2. High Fluorine (Cu-HF) Phase

Various solutions with select F/M ratios (1.5, 2, 2.5) were prepared. Copper acetate (8 mmol), hydrofluoric acid and ammonium hydroxide (OH/M ratio = 1) were added to DI water (40mL) and stirred for a few minutes. The solution has been transferred into a reaction vial with capacity of 90mL

and reacted at 80°C for 30 min in a microwave synthesis reactor. The final solutions were cooled down to room temperature and the blue precipitate was collected by centrifugation, washed several times with DI water and dried in an oven for 6 hours at 80°C.

2.2.3. Starting F/M ratio and phase purity

Because of the Jahn-Teller effect of Cu^{2+} ions, copper hydroxyfluorides compounds represent an interesting series due to tunability of the anionic ratio. In this respect, different synthesis with various starting HF/M ratio have been tried. It appeared that this ratio is a very relevant parameter to control the final composition. The results are reported in Table 1. Because HF is relatively weak acid ($\text{pK}_a(\text{HF}/\text{F}^-) = 3.2$), it is difficult to make a precise correlation between pH and the fluorine amounts in the medium. Taking into account that ammonia ($\text{pK}_a(\text{NH}_4^+/\text{NH}_3) = 9.2$) is a weak base, alternative studies using ammonium fluoride (for NH_4F at 0.1 M, $\text{pH} = 6.2$ and $\text{pH} = 7$ for $\text{NH}_4\text{F}/\text{Cu}$ ratio = 0.5-2) were done (Table S1), demonstrating a dominant pH effect. The pH value is correlated to the F/OH ratio directly in the medium and it appears as a crucial parameter for the synthesis of hydroxyfluorides. Furthermore, considering such concentration (Table S1), in a forthcoming paper, microwave-assisted hydrothermal synthesis reveals almost similar F contents as detected in Cu-LF but a different atomic arrangement.

The Cu-LF phase is pure after precipitation around $\text{pH}=6$ within a narrow existence domain, the amount of fluorine in $\text{Cu}(\text{OH})_{2-x}\text{F}_x$ being limited around the CP-2 sample (Table 1). The Cu-HF phase is stable on a broader pH range and it is easier to modulate the composition and access to different fluorine ratios, F varying from 0.95 ± 0.02 to 1.46 ± 0.02 . However, different F/OH ratio does not strongly affect the unit-cell parameters of the structure (Fig S1 and Table S2). The CP-2 and MW-2 compounds were selected for structural studies, named Cu-LF and Cu-HF, respectively.

Sample	Starting HF/Cu ratio	Starting pH	Identified Phases	F ⁻ content *	Final Composition**
CP-1	0.5	7	Cu(OH) _{2-x} F _x (Cu-LF) / Cu(OH) ₂	##	##
CP-2	1	6	Cu(OH) _{2-x} F _x (Cu-LF)	0.58(1)	Cu(OH) _{1.42} F _{0.58}
CP-3	1.5	5	No precipitate	##	##
MW-1	1	6	Cu(OH) _{2-x} F _x (Cu-LF + Cu-HF) / Impurities*	##	##
MW-2	1.5	5	Cu(OH) _{2-x} F _x (Cu-HF)	0.95(1)	Cu(OH) _{1.05} F _{0.95}
MW-3	2	4.7	Cu(OH) _{2-x} F _x (Cu-HF)	1.46(1)	Cu(OH) _{0.54} F _{1.46}
MW-4	3	4.7	Cu(OH) _{2-x} F _x (Cu-HF) / (NH ₄) ₂ CuF ₄	##	##

Table 1 : Hydroxyl-rich and Fluorine-rich phases obtained with different starting HF/Cu molar ratio. *F⁻ content determined by fluoride ion-selective electrode. **Cu content determined by ICP-AES, OH content by electroneutrality

3. Results and discussion

3.1. X-Ray diffraction analysis, long range order and anionic ordering/disordering.

3.1.1. XRD analysis and long range order.

Powder XRD data refinement and related structures are reported on Figure 1. Refined unit cell parameters and crystallite size, reliability factors, atomic positions and bond distances are reported on Table 1. Thanks to the fast kinetics during hydrolysis and fluorolysis of Cu²⁺ complexes at pH=6 (slightly acidic) and room temperature, a new phase with high symmetry and low F content (Cu(OH)_{1.42}F_{0.58}) was stabilized and crystallize with the Brucite network (*P-3m1*). It exhibits a well-marked 2D character. The XRD powder refinement (Figure XRD) shows the best reliability factors (Rp = 2.3 %, wRp = 3.4 % and R(Bragg) = 2.3 %, JANA 2006). The F molar content (determined by F titration using F specific electrode) can vary between 0.5 and 0.6 without affecting the structural features. The Cu (-3m site symmetry) local environment reveals the occurrence of 6 Cu-X (X=F, OH) equal bond lengths at 2.36 Å, much larger than those observed in βNi(OH)₂ (Ni-O = 2.13 Å) and Zn(OH)₂ (Zn-O = 2.27 Å), despite the Jahn-Teller effect of Cu²⁺. Then, F⁻ and OH⁻ anions, at low F content, remain randomly distributed around Cu²⁺ on the basis of XRD data analysis. Moreover, the platelet-shaped crystallites led to a preferential orientation along c-axis.

With low F content, surprisingly, the $\text{Cu}(\text{OH})_{1.42}\text{F}_{0.58}$ remains disordered with the absence of anionic ordering and a clear bi-dimensional character. The fast kinetics of reaction do not allow a long range anionic reorganization. The increase of F content leads to more complex results. The powder XRD patterns of two F-rich Cu hydroxyfluorides, $\text{Cu}(\text{OH})_{1.05}\text{F}_{0.95}$ and $\text{Cu}(\text{OH})_{0.54}\text{F}_{1.46}$ with a larger solubility limit than the previous one, were refined with the $P2_1/a$ hypothesis previously described for CuOHF^{16} . This result is not in agreement with the previous structure of $\text{Cu}(\text{OH})_{0.66}\text{F}_{1.33}$ ($P2_1/n$)¹⁶ on the basis of single crystal analysis which exhibit zig-zag chains in a 3D tunnel framework. The synthesis conditions with the precipitation at acidic pH followed by hydrothermal treatment at lower temperature are clearly different and should explain the structural differences. Almost similar unit-cell parameters were refined despite various F content. If the envelope of XRD patterns exhibits numerous similarities with the $P2_1/a$ model and despite correct reliability factors (Figure 1, table 2), a careful analysis shows that several peaks and shoulders are not so well refined, notably concerning (120) (021) ($\bar{2}01$) and ($\bar{1}21$) diffraction lines around 35° (2θ) region. Moreover, preferential orientation involving c axis was also taken into account. Furthermore, electron diffraction analysis was carried out but the powders are very sensitive under the electron beam. Only few observations were performed revealing the same zone axis and one should have to point out the rather high homogeneity of this sample. However, if the main spots ($20\bar{1}$), ($\bar{1}20$) or ($12\bar{1}$) are clearly associated to the monoclinic unit lines, 7 extra (commensurate) spots along ($44\bar{3}$) or ($\bar{5}22$) directions, leading to consider a commensurate superstructure. To solve and determine the super cell, more observations with other zone axis are necessary but unfortunately it was impossible because of the high sensitivity of the sample under the electron beam ; an effort which is beyond the scope of the current study. Although, the $P2_1/a$ model was not correct for F-rich compositions, this average monoclinic unit cell reflects globally the impact of a larger F content on $\text{Cu}(\text{OH})_{1-x}\text{F}_{1+x}$ structural features. Two anionic sites are reported and depending on the $\text{Cu}(\text{OH})_{1.04}\text{F}_{0.96}$ and $\text{Cu}(\text{OH})_{0.5}\text{F}_{1.5}$ compositions, (4+2) distorted octahedral sites corresponding mainly to $\text{Cu}(\text{OH})_3\text{F}_3$ and $\text{Cu}(\text{OH})_2\text{F}_4$ polyhedra respectively could be identified. In this case, the Cu site symmetry is sharply lowered and differs from the previous one with 4 shorter Cu-X bond lengths which vary between 1.94 Å and 2.00 Å whereas the 2 longer one's are between 2.28 Å and 2.36 Å. These values remind the Cu-F bond distances in distorted rutile- CuF_2 with the influence of OH groups leading to shorten the Cu-Cu distance from 3.30 Å in CuF_2 to 2.98 Å-3.18 Å in $\text{Cu}(\text{OH})_{1.05}\text{F}_{0.95}$. The hydroxyls and hydrogen bonds with Van Der Waals interactions between the layers which appears buckled, in competition with fluorine, contribute to the 2D character of this mixed anions system. Finally, a low limit (OH) or F content around 0.5 allows keeping an ordered/folded or disordered/unfolded 2D networks respectively.

The crystal structure of two Cu hydroxyfluorides have been previously well described in the literature¹⁶ from single crystal analysis. In CuOHF ($P2_1/a$ with $Z=4$) and $\text{Cu}(\text{OH})_{0.66}\text{F}_{1.33}$ (labelled $\text{Cu}_2(\text{OH})_3\text{F}_4$ $P2_1/n$ with $Z=2$), Cu^{2+} Jahn-Teller ($3d^9$) ions are stabilized in elongated octahedra (4 bond distances at 1.9-1.98 Å and 2 others ones at 2.3-2.34 Å). The network of CuOHF is strongly related to that observed in Layer Double Hydroxides (LDH) and Brucite structure with folded layers of edge sharing $\text{Cu}(\text{OH})_3\text{F}_3$ octahedra, interconnected by hydrogen bonds. When the F/OH atomic ratio increases, the structure of $\text{Cu}(\text{OH})_{0.66}\text{F}_{1.33}$ exhibits zig-zag chains with two kind of $\text{CuF}_4(\text{OH})_2$ distorted octahedra sharing edges as in CuOHF with Cu-Cu distances varying between 3.00 Å and 3.14 Å. It should be emphasized that the decrease of OH content and hydrogen bonds in $\text{Cu}(\text{OH})_{0.66}\text{F}_{1.33}$ contributes to reduce its 2D character. On the other hand, the OH-rich Cu phases have never been explored before this work. Actually, the $\text{Cu}(\text{OH})_2$ hydroxide crystallizes in orthorhombic symmetry ($\text{Cmc}21$) with Cu^{2+} occupying elongated pyramids ($\text{Cu-O} : 4 \times 1.96 \text{ \AA} + 2.35 \text{ \AA} + 2.9 \text{ \AA}$) in zig-zag chains with attenuated 2D character. Because of larger Cu-X bond distances, considering competitive bonds, shorter Cu-Cu distances at 2.95 Å is also expected. Elongated octahedra ($\text{Cu-F} : 4 \times 1.92 \text{ \AA} + 2 \times 2.30 \text{ \AA}$) with a weaker distortion is identified in CuF_2 and consequently a longer Cu-Cu distance around 3.30 Å.

In complement to the average structure details determined by traditional X-ray powder diffraction analysis, the local atomic environments were examined directly by PDF (pair distribution function) analysis. These structural considerations will have a strong impact on exchange interactions related to magnetic properties as well as crystal field effect and charge transfer band connected to optical absorption properties.

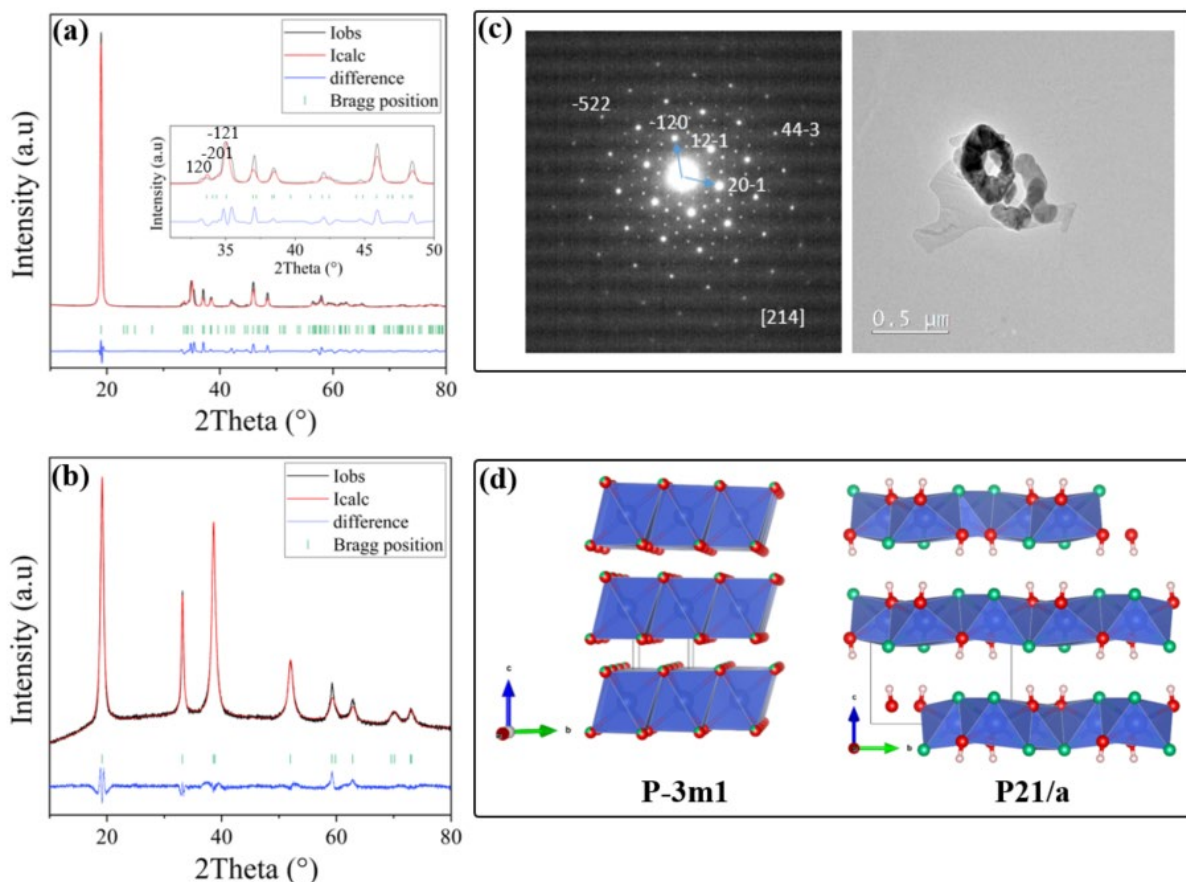


Fig. 1: Powder diffraction patterns of a) Cu-HF $P2_1/a$ phase, b) Cu-LF $P-3m1$ phase. c) Electron Diffraction pattern of Cu-HF $P2_1/a$ phase. d) Crystal structures obtained by Rietveld refinement.

Results of Rietveld refinement

Sample	Cu-HF	Cu-LF
Space group	$P12_1/a1$ (N°14) (C_{2h}^5)	$P-3m1$ (N°164) (D_{3d}^3)
a (Å)	5.260(3)	3.1175(6)
b (Å)	6.360(4)	
c (Å)	5.064(2)	4.634(1)
β (°)	112.92(1)	
V (Å ³)	156.82(6)	39.0(1)
Z	4	1
Crystallite size (nm)	19.4(2)	17.9(1)
Rp (%)	12.8	2.10
wRp (%)	19.73	2.86
R _{Bragg} (%)	5.45	2.27

Table 2: Structural parameters and reliability factors obtained from refinement of the two hydroxyfluorides using the X-ray powder diffraction data

Cu-HF $P2_1/a$		Cu-LF $P-3m1$	
Atom pair	Distance (Å)	Atom pair	Distance (Å)
Cu-F	1.9652(6)	6x Cu-O/F	2.357(5)
Cu-F	2.2832(3)	6x Cu-Cu	3.1175(3)
Cu-F	2.3557(3)		
Cu-O	1.9414(3)		
Cu-O	1.9536(6)		
Cu-O	2.0077(3)		
Cu-Cu	2.9882(5)		
2x Cu-Cu	3.0957(6)		
Cu-Cu	3.1384(6)		
2x Cu-Cu	3.1840(8)		

Table 3: Interatomic distances obtained from Rietveld refinements of XRD patterns of the Cu-HF ($P2_1/a$) and Cu-LF ($P-3m1$) phases.

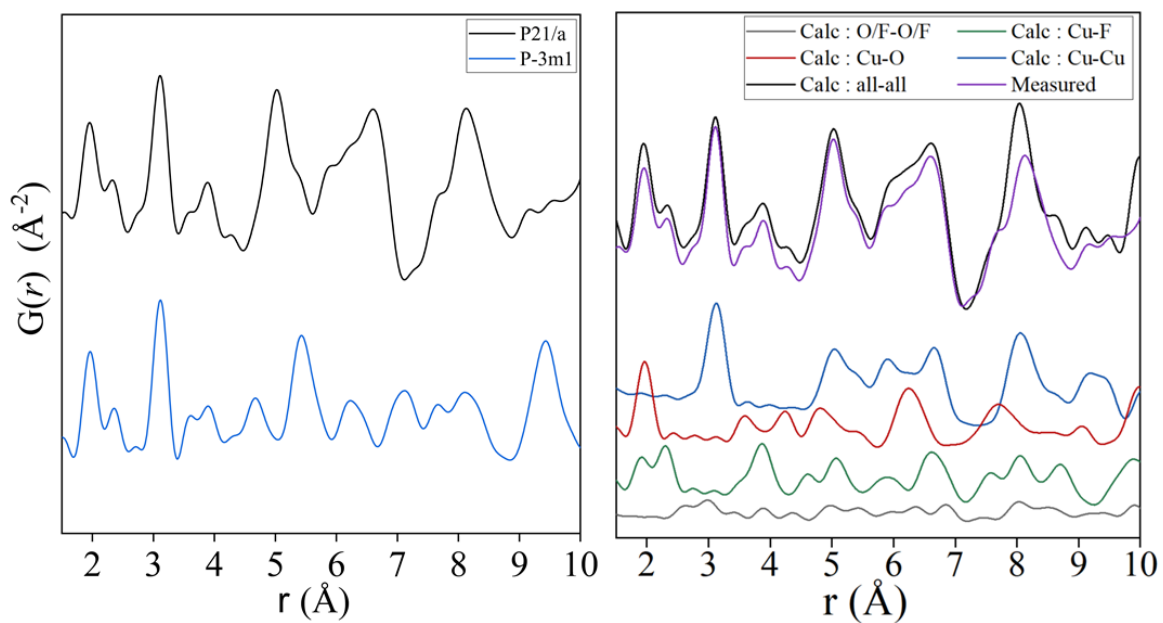


Figure 2 : a) X-Ray pair distribution function data of the two Cu-HyF phases . b) Comparison between measured and simulation (complete and partial) plot of interatomic bonding for the $P2_1/a$ phase.

Atom pair	$P2_1/a$: Distance (Å)	$P-3m1$: Distance (Å)	Attribution
4 x Cu-A + 2x Cu-A	1.97 + 2.33	1.97 + 2.33	First octahedron
Cu-Cu	3.10	3.10	Intra-sheet bond
Cu-Cu	5.04	5.42	Inter-sheet bond

Table 4 : Attribution of selected atomic pairs to the local structure of the two hydroxyfluorides.

3.1.2 PDF analysis and short range order : competitive bonds between the slabs and into the sheets.

The experimental and simulated PDF data and simulation considering $P2_1/a$ hypothesis are represented in Figure 2 and data are reported on Table3. The X-ray pair distribution function $G(r)$ data in Fig.2 was collected to observe the local structure-bonding environment in $\text{Cu}(\text{OH})_{1.42}\text{F}_{0.58}$ ($P-3m1$) and $\text{Cu}(\text{OH})_{1.05}\text{F}_{0.95}$ ($P2_1/a$). The PDF plot of known $P2_1/a$ phase has been simulated to facilitate the attribution of the different atom pair distances. The agreement with the $P2_1/a$ model for $\text{Cu}(\text{OH})_{1.05}\text{F}_{0.95}$ composition is almost perfect, confirming the rather good representation of this structure at short range ($< 7 \text{ \AA}$). Beyond 7 \AA , clear differences with $P2_1/a$ model appear then showing another atomic organization at long range as confirmed by electron diffraction investigation. At very short range ($< 4 \text{ \AA}$), the atomic pair peaks are similar between the two hydroxyfluorides. The first octahedron appears with 4 short bonds at 1.97 \AA and 2 longer bonds at 2.33 \AA . This geometry is characteristic of the Jahn-Teller distortion and is observed in CuF_2 (4+2 bond distances) but not in $\text{Cu}(\text{OH})_2$ (4+1 bond distances). This effect is noticeable with long range X-ray diffraction analysis of the average structure of $\text{Cu}(\text{OH})_{1.05}\text{F}_{0.95}$, the so called Cu-HF. However, although average long range structural analysis of the $\text{Cu}(\text{OH})_{1.42}\text{F}_{0.58}$ (the so-called Cu-LF) network show 6 equal Cu-X bond-lengths, direct probing of the short range order by PDF method shows a clearly observed short range Jahn-Teller distortion with almost the same distribution (4+2) as detected for Cu-HF phase. Concerning the anionic ordering and the preferential occupancy of F vs OH groups around the CuX_6 octahedron, calculations using the Brown & Altermatt model²² predict longer axial Cu-F bonds where the hydroxyl ions are more stable forming short equatorial bonds.

Both phases have also similar Cu-Cu distances into the sheets at 3.10 \AA . Actually, 6 Cu-Cu intra-layer distances can be evaluated on the basis of XRD data refinement ($P2_1/a$) between 2.98 \AA and 3.19 \AA . These values are between those calculated for $\text{Cu}(\text{OH})_2$ (2 shorter Cu-Cu at 2.95 \AA) and for CuF_2 (2 shorter Cu-Cu at 3.30 \AA). The other shell around 4 \AA is related to longer Cu-O/F distances and a clear intensity change appears between Cu-LF and Cu-HF and should be connected to the larger content of F anions within the sheet.

Finally, the biggest difference between the two compositions concerns the Cu-Cu shells just after 5 Å involving Cu atoms in two different slabs. The High-Fluorine compound exhibits shorter inter-sheet bonding (5.04 Å) than the low fluorine one (5.42 Å). The interslab space as well as the M-X vs M-M competitive bonds within the sheets of 2D structures provides considerable information. In M(OH)X structures (with X = F, Cl, O) and especially hydroxyfluorides, this interslab space is expected to be correlated to the strength of the hydrogen bonding and Van De Waals interactions^{23–25}. The Cu-HF has an average of one fluorine atom per octahedron more than the Cu-LF structure. This fluorine atom exhibits stronger hydrogen bindings (O-H---F) than the oxygen due to its much larger electronegativity.

At a local structural scale in Cu-LF phase, within the Cu octahedron environment, a Jahn-Teller distortion is clearly evidenced, which then disappears on long range due to the random distribution of anions in the vicinity of Cu²⁺ which leads to destruction of this local electronic effect. When the F content increases in Cu-HF compound, resulting in a greater fraction of Cu-F ionic bonds and a clearer distribution of charge, two anionic sites can be distinguished and the Cu²⁺ Jahn-Teller is detected with a long-range order.

3.2. Spectroscopic analysis of the two Cu-HyF structures

3.2.1. Raman investigation

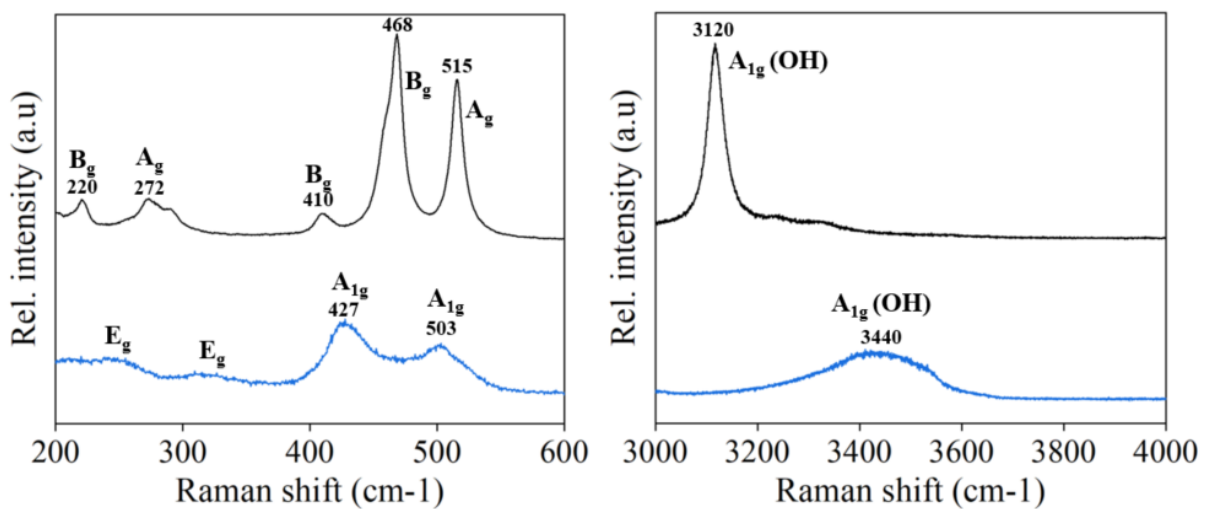


Figure 3: Raman spectra of the two copper hydroxyfluorides: Cu-LF (Blue) and Cu-HF (Black). The Raman active modes were labelled.

The Cu-LF Raman spectrum exhibits very broad peaks, in agreement with a poorly ordered long-range structure. This observation is consistent with previous results from X-ray analysis. On the basis of the point group D_{3d} , deduced from $P-3m1$ space group (Cu-LF), in the case of an ideal Brucite structure with Cu(OH,F)₂ formulation (meaning that the local cluster has the full symmetry of the

crystallographic site $-3m$, *i.e.* D_{3d} in Schoenflies notation[@]), there are only 4 Raman active modes¹ $\Gamma(\text{Raman}, D_{3d}) = 2A_{1g} + 2E_g$ ²⁶. Two modes are related to the OH in-phase stretching along the c axis (A_{1g} : expected $\approx 3650 \text{ cm}^{-1}$) and the in-phase bending perpendicular to the c axis (E_g : expected $\approx 725 \text{ cm}^{-1}$). The two other Raman modes correspond respectively to the $\text{Cu}(\text{OH},\text{F})_2$ in-phase stretching along the c axis (A_{1g} : expected $\approx 420\text{-}440 \text{ cm}^{-1}$) and to the $\text{Cu}(\text{OH},\text{F})_2$ in-phase bending perpendicular to the c axis (E_g : expected $\approx 240\text{-}280 \text{ cm}^{-1}$). However, the D_{3d} hypothesis remains partially incorrect because of the occurrence of two anions F^- and OH^- in the vicinity of Cu^{2+} . X-ray diffraction patterns give only a time average of the Cu cluster while an optical spectroscopy like Raman scattering is able to see the instantaneous structure of the concerned cluster if the dynamic/time life of that cluster falls in the range of nucleus motion, *i.e.* from long time up to the picosecond range. For shorter time life, typically the femtosecond range, Raman spectroscopy will see an average dynamical structure, as X-ray diffraction does. Hence, we expect a broadening of the band and a partial release of the vibrational selection rules towards a vibrational-density-of-state (V-Dos), since the vibrational modes are not able to achieve full cycles (they are essentially dissipative as in a glass). Consequently, in the time average D_{3d} description we may expect very fast radial density fluctuations meaning that the observed Raman bands will come essentially from stretching modes. Since all the stretching modes are along the c axis, they are expected to be of A type. The first type is A_{1g} , which is always Raman allowed whatever the dynamic scaling. The second irreducible representation is A_{2u} that is normally only IR-active, but here there is an induced Raman-active polarizability contribution arising from the very fast dynamic of the two anions that disymmetrize the Cu-X cluster. On the other hand, E_g type modes are expected to give weak (or not resolved) intensities in such scheme; this is probably even true for the E_u type.

So, for the Cu-LF structure (Figure 3), we assign the broad band $\approx 3440 \text{ cm}^{-1}$ as the expected OH^- in-phase stretching along the c axis (A_{1g}), but with a weakening of the bond strength due to the influence/exchange of F. Following the proposed dynamical model, we expect also the OH^- out-of-phase stretching modes (A_{2u}) as a weak peak and shoulder in the high frequency side, which is indeed not resolved since these two OH^- in-phase and out-of-phase stretching modes exhibit currently a weak frequency splitting ($< 30 \text{ cm}^{-1}$). In the low frequency range, we assign the band at 427 cm^{-1} to the Cu-X in-phase stretching (ν_s) along the c axis (A_{1g}). Again, the frequency is lower than in the Brucite structure^{26,27} probably because of the weakening of the mixed Cu-X bonds. At higher frequency, the normally Raman inactive A_{2u} corresponding to Cu-X out-of-phase stretching (ν_{as}) along the c axis is assigned to the mode at 503 cm^{-1} . The associated intensity is weaker than the Raman-allowed A_{1g} mode at 427 cm^{-1} . Note that we ruled out the E_g mode corresponding to the OH vibration because first it is

[@]Note these Raman modes are intrinsically symmetric with the inversion center symmetry operation

better expected in the 600-725 cm^{-1} range than at 503 cm^{-1} and second because it is expected to involve only weak radial fluctuations of the polarizability with not resolved band intensity

For the Cu-HF structure, we have to consider the point group C_{2h} deduced from $P2_1/a$ space group. The $P2_1/a$ structure contains four formula per unit cell ($Z=4$), so we expect now 24 Raman modes with either A_g or B_g symmetries. The interpretation of the corresponding Raman spectrum is not obvious in this case. However, a few points can be addressed. All the Raman bands show a classical profile with spectral width at half-maxima ca 10-20 cm^{-1} , indicating now that this lower-symmetry structure does not exhibit any more a very fast dynamic as seen in the prototype $P-3m1$ structure.

Furthermore, the higher wavelength of A_g mode in Cu-HF than A_g mode in Cu-LF, reflects the more rigid octahedral sites in Cu-HF. The spectra of the Cu-HF- $P2_1/a$ looks like the ones described in the literature^{16,23}. However, one difference can be noticed as the occurrence of a shoulder around the band at 468 cm^{-1} . It shows that the $P2_1/a$ space group is not the right structural model. Now comparing the two structures of Cu-LF and Cu-HF hydroxyfluorides, the $P2_1/a$ network exhibits a less marked 2D character than the $P-3m1$ structure. A bending or folding phenomenon is indeed clearly evidence in the Cu-HF compound. The frequency increase of the Cu-X mode from 503 cm^{-1} in Cu-LF to 515 cm^{-1} in Cu-HF could reflect the increase of octahedron stiffness in Cu-HF. Moreover, for Cu-HF, the characteristic O-H stretching mode is observed around 3120 cm^{-1} , whereas the frequency of this mode is usually higher for other hydroxyfluorides materials, for instance around 3306 cm^{-1} for $\text{Cu}(\text{OH})_{0.66}\text{F}_{1.33}$ ¹⁶ and 3500-3300 cm^{-1} for $\text{Zn}(\text{OH})\text{F}$ ²⁸. As explained by Giester et al.¹⁶, this weaker O-H stretching can be the consequence of stronger hydrogen bonding. The Cu-LF phase shows a flat band at still higher frequency at 3440 cm^{-1} . Such a higher frequency should be also due to the occurrence of F^- ions in interactions with H atoms. This much higher shift for the latter shows weaker hydrogen bonding than the Cu-HF phase and is in good agreement with higher inter-layer distance shown by PDF investigations. By consequence, the Cu-HF has more interactions between the layers and better cohesion but also considering competitive bonds, lower Cu-Cu interactions within the slabs.

3.2.2 UV-Visible-NIR characterization

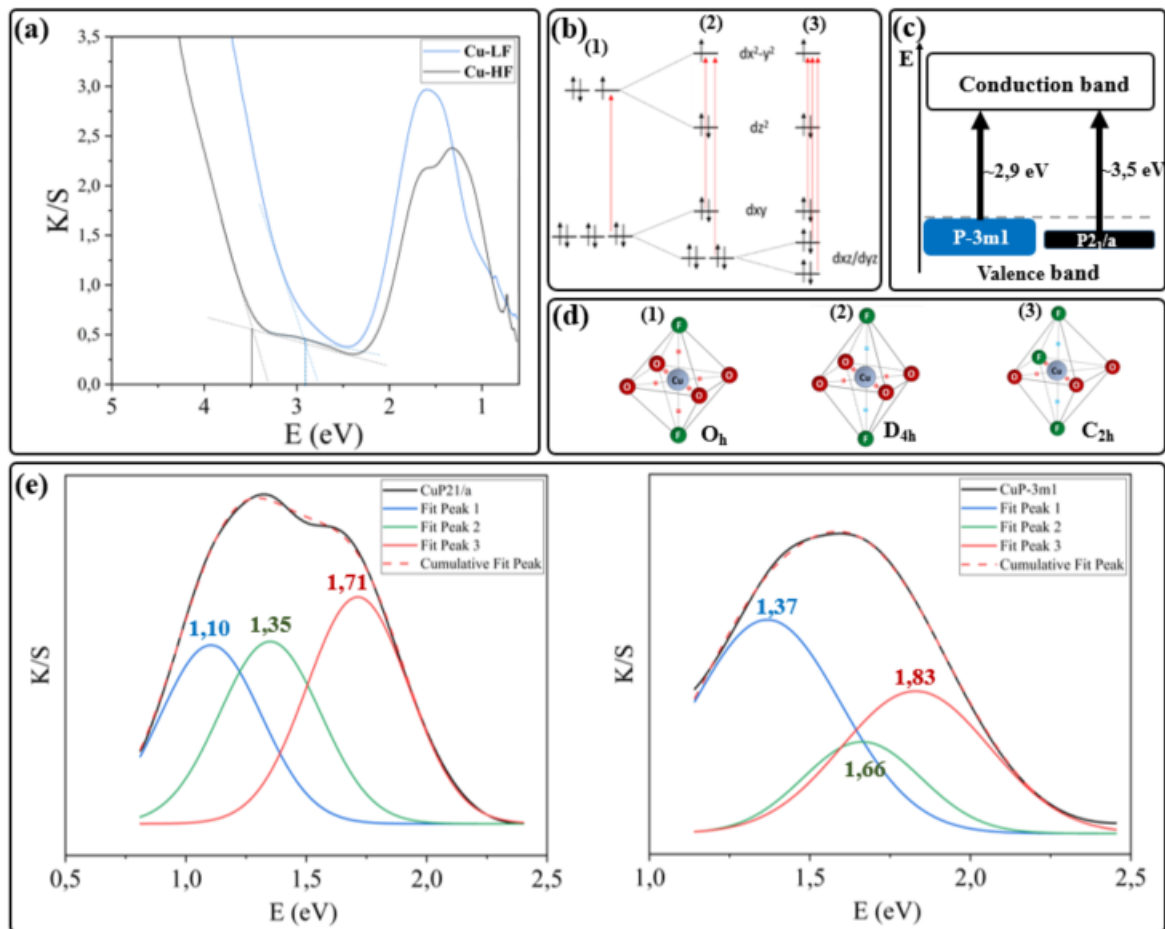


Figure 4 : a) UV-Visible-NIR spectra of the two Cu-HyF, b) Atomic orbitals of $3d^9$ Cu^{2+} with different distortions and electronic transitions, c) Scheme of valence and conduction bands related to the two Cu phases, d) $\text{Cu}(\text{O})_4\text{F}_2$ and $\text{Cu}(\text{O})_3\text{F}_3$ octahedra with different distortions, e) Peak deconvolution of d-d bands for the two hydroxyfluorides

UV-Vis-NIR absorbance curves (Kubelka-Munk transforms) are superimposed for the two hydroxyfluorides Cu-HF and Cu-LF in Fig 4.a. The optical band gap ($\text{O}(2p) \rightarrow \text{Cu}(\sigma_{x^2-y^2})$) estimated by tangential methods strongly change from 2.9 eV for Cu-LF to 3.5 eV for Cu-HF (Figure 4.a and c). The higher content of less electronegative OH groups than F in Cu-LF contributes to decrease the band gap. The envelopes of d-d transitions are centered around 1.5 eV for Cu-LF and 1.3 eV for Cu-HF. They are related to Jahn-Teller Cu^{2+} in elongated octahedral site. Furthermore, the intensity of d-d band at 1.5 eV in Cu-LF is higher and the envelope slightly shifts to higher energy. The deconvolution in Fig 4.e allows to fit the experimental curves by the identification of 3 Gaussian curves with almost identical Full Width at Half Maximum (FWHM) (~ 0.21 eV) corresponding to the 3 following d-d electronic transitions : $d_{xz}/d_{yz} - d_{x^2-y^2}$ at 1.83 eV / 1.71 eV for Cu-LF/Cu-HF > $d_{yz}/d_{xz} - d_{x^2-y^2}$ at 1.66 eV / 1.35 eV for

Cu-LF/Cu-HF $> d_{xy} - d_{x^2-y^2}$ at 1.37 eV / 1.10 eV for Cu-LF/Cu-HF. The crystal field splitting corresponding to $d_{xz}/d_{yz} - d_{x^2-y^2}$ transition roughly increases of 0.1 eV for Cu-LF with the higher OH content in agreement with the spectrochemical series. Then the $d_{xy}-d_{x^2-y^2}$ as well as the $d_{yz}/d_{xz}-d_{x^2-y^2}$ transitions shift at lower energy for Cu-HF compound. We can then deduce that $d_{xz}-d_{yz}$ (0.36 eV for Cu-HF vs 0.17 eV for Cu-LF) orbitals energy difference is higher for Cu-HF compound. The larger splitting of $d_{xz}-d_{yz}$ orbitals is in agreement with the C_{2h} point group identified for Cu-HF in comparison with the average D_{3d} point group for Cu-LF (Fig. 4.e). The F content increase contributes towards a symmetry lowering, a rise of $d_{xz}-d_{yz}$ degeneracy lifting and a decrease of crystal field energy splitting.

3.3. Thermogravimetric measurements and evidence of redox phenomena

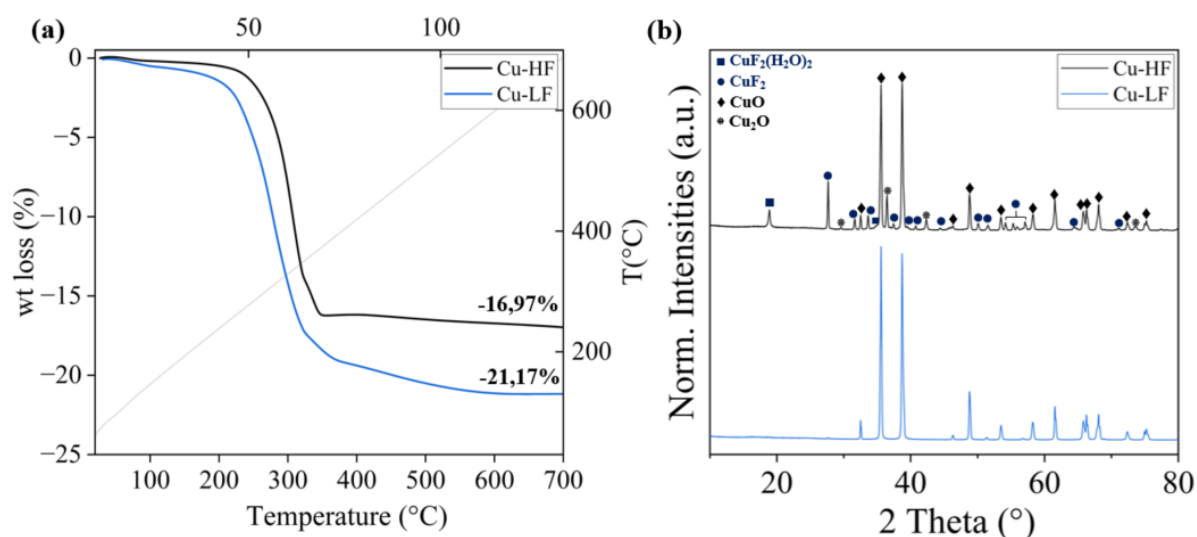


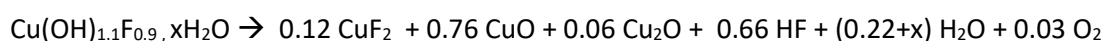
Figure 5 : (a) Thermogravimetric analysis (TGA) under argon of Cu-HF and Cu-LF samples with 10°C/min heating rate. (b) X-Ray analysis of the decomposition products after TGA.

Fig.5(a) shows the thermogravimetric analysis under argon of the two Cu hydroxyfluorides. The Cu-LF compound is less stable than the more fluorinated one. This result was predictable taking into account that this structure is poorly organized and has less cohesive interlayer with weaker hydrogen bindings. Moreover, we outlined a slight structural water loss after $T > 100^{\circ}\text{C}$ for Cu-LF compound, in good agreement with the higher hydroxyl content between the slabs. The two phases show similar thermal behavior with an S-shape curve, a more abrupt slope and a more pronounced plateau for Cu-HF sample, but the Cu-LF compound loses 4% more matter. This difference can be explained by the decomposition products X-ray analysis (Fig.5.b). At the end of the thermal decomposition of the Cu-LF, only CuO remains leading to consider the $0.6 \text{ HF} + 0.4 \text{ H}_2\text{O}$ evolution with a theoretical weight loss equal to 19.5% in agreement with of the 19.5% experimental weight loss

deduced from 21.2% (-1.7% , water departure at $T < 200^{\circ}\text{C}$). Taking into account the chemical composition and the OH/F partial ordering already discussed in the above parts, the Cu-LF / $\text{Cu}(\text{OH})_{1.4}\text{F}_{0.6}$ hydroxyfluoride layout mainly $\text{Cu}(\text{OH})_4\text{F}_2$ octahedron with fluoride ions located on the apical site of the distorted octahedron at 2.33 Å, caused by the Cu^{2+} J.T distortion. The Cu-F bond is then very weak, but fluorine also strongly interacts with a neighboring hydrogen, affecting the hydrogen bonding and Vander Waals interactions. By consequence, a large HF departure in association with H_2O was observed. The simple reaction of thermal decomposition of Cu-LF compound is then:



In the other hand, the Cu-HF composition ($\text{Cu}(\text{OH})_{1.05}\text{F}_{0.95}$) leads, in a first approximation, to $\text{Cu}(\text{OH})_3\text{F}_3$ octahedrons. Here, the octahedron has two long Cu-F bondlengths (2.33 Å) caused by the J.T distortion but also one fluoride ion within the plane, with a short Cu-F bondlength (1.97 Å). Consequently, as the previous hexagonal cell, in this monoclinic network, the two fluoride ions (F⁻) in the apical sites will react with the protons (H⁺) within the interslab space, allowing the formation of 0.66 HF. However in the Cu-HF sample, the final product after decomposition contains also hydrated and dehydrated copper difluoride. Thus, the F⁻ ions within the basal plane with shorter Cu-F bondlengths allow the stabilization of CuF_2 phases (approximately 15 % molar) in the final product. Leaving the sample under air leads to the formation of a small amount of copper fluoride dihydrate $\text{CuF}_2 \cdot 2\text{H}_2\text{O}$. More surprisingly, Cu_2O (approximately 5 % molar) is noticeable in the final product, traducing a reduction from Cu(II) to Cu(I). The found equation for the thermal decomposition of Cu-HF is close to:



In these experimental conditions, the theoretical weight loss around 18.2 % converges to the experimental one equal to 17%. In cuprite Cu_2O framework, short Cu-O and Cu-Cu bondlengths are identified at 1.85 Å and 3.01 Å respectively. Thus, the formation of Cu_2O and the unexpected reduction process starting at $T = 320^{\circ}\text{C}$ under Ar of Cu-HF (on the basis of Ellingham diagram) is the consequence of the shorter Cu-O bonding around 1.94 Å with stronger orbitals $\text{Cu } \sigma(x^2-y^2) - \text{O } p(x,y)$ overlapping as well as stronger Cu-Cu interactions detected at 2.99 Å in the pseudo monoclinic ($P2_1/a$) unit cell. Taking into account this redox phenomena and associated charge transfer as well as the occurrence of various chemical bonding Cu-F/Cu-OH involving various acidic-basic behavior, this latter hydroxyfluorides should exhibit interesting (electro)catalytic properties or could be used as electrodes in alkaline batteries.

4. Conclusions

In summary, the initial fluorine amount and the pH of the solution during the precipitation step followed by hydrothermal treatment at 80°C in several cases is determining in the stabilization of different copper hydroxyfluorides. It leads to high or low fluorine content stabilized in two different structures. Cu-LF compound with low fluorine content ($\text{Cu}(\text{OH})_{1.4}\text{F}_{0.6}$) crystallizes with brucite structure ($P-3m1$) with a random distribution of OH^- and F^- anions at the vertices of Cu^{2+} octahedral site. The domain of existence is very narrow and vary between $\text{F}_{0.5}$ and $\text{F}_{0.6}$. However, the pair distribution function (PDF) analysis reveals at short range the occurrence of (4+2) distorted octahedral site ($4 \times 1.97 \text{ \AA} + 2 \times 2.33 \text{ \AA}$) associated to the Cu^{2+} Jahn-Teller effect. In a forthcoming paper, we will show how microwave-assisted hydrothermal synthesis allows preparing new phases with almost similar F/OH molar ratio as Cu-LF compounds but exhibiting anionic ordering. The other phase Cu-HF with a higher fluorine content and a larger domain of existence (varying between the $\text{Cu}(\text{OH})_{1.05}\text{F}_{0.95}$ and $\text{Cu}(\text{OH})_{0.54}\text{F}_{1.46}$ compositions) adopts an average monoclinic unit cell ($P2_1/a$) with distorted $\text{Cu}(\text{OH})_3\text{F}_3$, $\text{Cu}(\text{OH})_2\text{F}_4$ and $\text{Cu}(\text{OH})\text{F}_5$ octahedra. The Cu-F/O bondlengths in the basal plane vary between 1.96 Å and 2.00 Å and the apical sites between 2.28 Å and 2.36 Å. The PDF analysis is in good agreement with the long range order detected in the $P2_1/a$ hypothesis. Moreover if the Cu-Cu intra-sheet distances do not change at all between Cu-LF and Cu-HF, a large difference is observed for the Cu-Cu interslab space evolving from 5.04 Å in Cu-HF to 5.42 Å in Cu-LF. The higher the fluorine content, the stronger the hydrogen bonding and the lower the interslab space. By Raman spectroscopy, the $\nu_{(\text{OH})}$ stretching mode (A_{1g}) are identified as a large and flat peak at high frequency for Cu-LF whereas a narrower Raman peak appear at lower frequency for Cu-HF. The random distribution of F^- and OH^- anions in the vicinity of Cu^{2+} explains the low intensity of Raman peaks in Cu-LF sample. Furthermore, the two structural hypothesis, $P-3m1$ for Cu-LF and $P2_1/a$ for Cu-HF compounds is in good agreement with the number of Raman peaks in low frequency region.

UV-Vis-NIR spectra show a large decrease around 0.6 eV of the optical band gap of Cu-LF hydroxyfluoride due to the decrease of F/OH molar ratio. Moreover, the red shift of d-d transitions in Cu-HF show the increase of crystal field splitting in Cu-LF around 0.1 eV and the raise of d_{xz} - d_{yz} orbital splitting in Cu-HF (around 0.2 eV) in good agreement with the rise of F content and the change of point group symmetry from D_{3d} to C_{2h} . Finally, it is worth outlining that the raise of F amount in this Cu hydroxyfluoride series lead to a drastic different thermal behavior. In Cu-HF sample, the Cu^{2+} - Cu^+ reduction is detected with the major formation of CuO but also CuF_2 and Cu_2O whereas for Cu-LF, only CuO is identified at $T > 300^\circ\text{C}$. The formation of Cu^+ is quite unusual at this temperature under Ar and shows that these mixed anions compounds should have promising catalytic or electrocatalytic properties. The occurrence of $\text{Cu}(\text{OH})_3\text{F}_3$, $\text{Cu}(\text{OH})_2\text{F}_4$ and $\text{Cu}(\text{OH})\text{F}_5$ polyhedra detected in Cu-HF with

competitive bonds in the vicinity of Cu^{2+} is in favor of the O-Cu electronic transfer and the reduction process. Stabilizing such octahedra in new mixed anions compounds will be a key feature to enhance catalytic or electrocatalytic properties.

Associated Content

Supporting information

Table S1 showing Hydroxyl-rich phases obtained with different starting $\text{NH}_4\text{F}/\text{Cu}$ molar ratio. *F-content determined by determined by fluoride ion-selective electrode. **Cu content determined by ICP-AES, OH content by electroneutrality. Table S2 showing Full pattern profile matching refinement parameters of two Cu-HF compositions corresponding to figure S1. Table S3 showing Atomic positions of Cu-LF and Cu-HF phases, refined from X-ray diffraction for Cu-LF, fixed from literature¹⁶ for $\text{P2}_1/\text{a}$. Figure S1 showing Full pattern profile matching refinement of two Cu-HF compositions: a) MW-2 (b) MW-3.

Acknowledgments

The authors would like to thank the French National Research Agency for the financial support (ANR FluHOMat project, ref ANR-21-CE08-0020-03)

References

- (1) Oliva, P.; Leonardi, J.; Laurent, J. F.; Delmas, C.; Braconnier, J. J.; Figlarz, M.; Fievet, F.; Guibert, A. de. Review of the Structure and the Electrochemistry of Nickel Hydroxides and Oxy-Hydroxides. *Journal of Power Sources* **1982**, *8* (2), 229–255. [https://doi.org/10.1016/0378-7753\(82\)80057-8](https://doi.org/10.1016/0378-7753(82)80057-8).
- (2) Aghazadeh, M.; Ghaemi, M.; Sabour, B.; Dalvand, S. Electrochemical Preparation of α - $\text{Ni}(\text{OH})_2$ Ultrafine Nanoparticles for High-Performance Supercapacitors. *J Solid State Electrochem* **2014**, *18* (6), 1569–1584. <https://doi.org/10.1007/s10008-014-2381-7>.
- (3) Cheng, Y.; Zhang, Q.; Fang, C.; Guo, S. CVD-Synthesis of MCMB/CNTs Hybrids with Low Specific Surface Area for Supercapacitors. *J. Electrochem. Soc.* **2017**, *164* (9), A1845–A1851. <https://doi.org/10.1149/2.0691709jes>.
- (4) Tang, P.; Feng, Y.; Li, D. Facile Synthesis of Multicolor Organic–Inorganic Hybrid Pigments Based on Layered Double Hydroxides. *Dyes and Pigments* **2014**, *104*, 131–136. <https://doi.org/10.1016/j.dyepig.2013.12.012>.
- (5) Lee, Y.-H.; Park, J.-Y.; Ahn, K.-S.; Sung, Y.-E. MnO_2 Nanoparticles Advancing Electrochemical Performance of $\text{Ni}(\text{OH})_2$ Films for Application in Electrochromic Energy Storage Devices. *Journal of Alloys and Compounds* **2022**, *923*, 166446. <https://doi.org/10.1016/j.jallcom.2022.166446>.

- (6) Hou, C.-C.; Wang, C.-J.; Chen, Q.-Q.; Lv, X.-J.; Fu, W.-F.; Chen, Y. Rapid Synthesis of Ultralong Fe(OH)₃:Cu(OH)₂ Core–Shell Nanowires Self-Supported on Copper Foam as a Highly Efficient 3D Electrode for Water Oxidation. *Chem. Commun.* **2016**, 52 (100), 14470–14473. <https://doi.org/10.1039/C6CC08780A>.
- (7) Lawson, K.; Wallbridge, S. P.; Catling, A. E.; Kirk, C. A.; Dann, S. E. Determination of Layered Nickel Hydroxide Phases in Materials Disordered by Stacking Faults and Interstratification. *J. Mater. Chem. A* **2023**, 11 (2), 789–799. <https://doi.org/10.1039/D2TA07655A>.
- (8) Rajamathi, M.; Vishnu Kamath, P.; Seshadri, R. Polymorphism in Nickel Hydroxide: Role of Interstratification. *J. Mater. Chem.* **2000**, 10 (2), 503–506. <https://doi.org/10.1039/a905651c>.
- (9) Kageyama, H.; Hayashi, K.; Maeda, K.; Attfield, J. P.; Hiroi, Z.; Rondinelli, J. M.; Poeppelmeier, K. R. Expanding Frontiers in Materials Chemistry and Physics with Multiple Anions. *Nat Commun* **2018**, 9 (1), 772. <https://doi.org/10.1038/s41467-018-02838-4>.
- (10) Wu, T.; Jiang, X.; Wu, C.; Hu, Y.; Lin, Z.; Huang, Z.; Humphrey, M. G.; Zhang, C. Ultrawide Bandgap and Outstanding Second-Harmonic Generation Response by a Fluorine-Enrichment Strategy at a Transition-Metal Oxyfluoride Nonlinear Optical Material. *Angew Chem Int Ed* **2022**, 61 (26), e202203104. <https://doi.org/10.1002/anie.202203104>.
- (11) Eom, T.-Y.; Cho, M.; Song, K.-Y.; Suh, S.-J.; Park, J.-S.; Lee, H.-J. Novel Co(OH)F/Zn(OH)F Heterostructures for Acetone Gas Sensor Applications: Materials Synthesis, Characterization, and Sensor Performance Evaluation. *Sensors and Actuators B: Chemical* **2022**, 356, 131377. <https://doi.org/10.1016/j.snb.2022.131377>.
- (12) Crichton, W. A.; Parise, J. B.; Müller, H.; Breger, J.; Marshall, W. G.; Welch, M. D. Synthesis and Structure of Magnesium Hydroxide Fluoride, Mg(OH)F: A Topological Intermediate between Brucite- and Rutile-Type Structures. *Mineral. mag.* **2012**, 76 (1), 25–36. <https://doi.org/10.1180/minmag.2012.076.1.25>.
- (13) Serier, H.; Gaudon, M.; Demourgues, A.; Tressaud, A. Structural Features of Zinc Hydroxyfluoride. *Journal of Solid State Chemistry* **2007**, 180 (12), 3485–3492. <https://doi.org/10.1016/j.jssc.2007.10.007>.
- (14) Yahia, H. B.; Shikano, M.; Kobayashi, H.; Avdeev, M.; Liu, S.; Ling, C. D. Synthesis and Characterization of the Crystal Structure and Magnetic Properties of the Hydroxyfluoride MnF_{2-x}(OH)_x (x ~ 0.8). *Phys. Chem. Chem. Phys.* **2013**, 15 (31), 13061. <https://doi.org/10.1039/c3cp50740h>.
- (15) Guo, Y.; Wang, C.; Cui, H.; Wang, M.; Sun, T.; Tang, Y. Net-Stacked Hierarchical CdOHF Architectures: Controllable Synthesis and Visible-Light Driven Photocatalytic Performance. *CrystEngComm* **2021**, 23 (41), 7334–7339. <https://doi.org/10.1039/D1CE01154E>.
- (16) Giester, G.; Libowitzky, E. Crystal Structures and Raman Spectra of Cu(OH)F and Cu₃(OH)₂F₄. *Zeitschrift für Kristallographie - Crystalline Materials* **2003**, 218 (5), 351–356. <https://doi.org/10.1524/zkri.218.5.351.20735>.
- (17) Kurzydłowski, D. The Jahn-Teller Distortion at High Pressure: The Case of Copper Difluoride. *Crystals* **2018**, 8 (3), 140. <https://doi.org/10.3390/cryst8030140>.
- (18) Oswald, H. R.; Reller, A.; Schmalle, H. W.; Dubler, E. Structure of Copper(II) Hydroxide, Cu(OH)₂. *Acta Crystallogr C Cryst Struct Commun* **1990**, 46 (12), 2279–2284. <https://doi.org/10.1107/S0108270190006230>.

- (19) Petříček, V.; Dušek, M.; Palatinus, L. Crystallographic Computing System JANA2006: General Features. *Zeitschrift für Kristallographie - Crystalline Materials* **2014**, *229* (5), 345–352. <https://doi.org/10.1515/zkri-2014-1737>.
- (20) Juhás, P.; Davis, T.; Farrow, C. L.; Billinge, S. J. L. PDFgetX3 : A Rapid and Highly Automatable Program for Processing Powder Diffraction Data into Total Scattering Pair Distribution Functions. *J Appl Crystallogr* **2013**, *46* (2), 560–566. <https://doi.org/10.1107/S0021889813005190>.
- (21) Farrow, C. L.; Juhas, P.; Liu, J. W.; Bryndin, D.; Božin, E. S.; Bloch, J.; Proffen, T.; Billinge, S. J. L. PDFfit2 and PDFgui: Computer Programs for Studying Nanostructure in Crystals. *J. Phys.: Condens. Matter* **2007**, *19* (33), 335219. <https://doi.org/10.1088/0953-8984/19/33/335219>.
- (22) Brown, I. D.; Altermatt, D. Bond-Valence Parameters Obtained from a Systematic Analysis of the Inorganic Crystal Structure Database. *Acta Crystallogr B Struct Sci* **1985**, *41* (4), 244–247. <https://doi.org/10.1107/S0108768185002063>.
- (23) Tian, H.; Wang, Y.; Zhang, J.; Ma, Y.; Cui, H.; Cui, Q.; Ma, Y. Compression Behavior of Copper Hydroxyfluoride CuOHF as a Case Study of the High-Pressure Responses of the Hydrogen-Bonded Two-Dimensional Layered Materials. *J. Phys. Chem. C* **2019**, *123* (41), 25492–25500. <https://doi.org/10.1021/acs.jpcc.9b07433>.
- (24) He, X.; Kagi, H.; Komatsu, K.; Nakano, S. Compressibility and Blue-Shifting O–H Stretching Bands of Magnesium Hydroxyfluoride Mg(OH)F up to 20 GPa. *Journal of Solid State Chemistry* **2021**, *303*, 122449. <https://doi.org/10.1016/j.jssc.2021.122449>.
- (25) Friedrich, A.; Wilson, D. J.; Haussühl, E.; Winkler, B.; Morgenroth, W.; Refson, K.; Milman, V. High-Pressure Properties of Diaspore, AlO(OH). *Phys Chem Minerals* **2007**, *34* (3), 145–157. <https://doi.org/10.1007/s00269-006-0135-5>.
- (26) Lutz, H. D.; Möller, H.; Schmidt, M. Lattice Vibration Spectra. Part LXXXII. Brucite-Type Hydroxides M(OH)₂ (M = Ca, Mn, Co, Fe, Cd) — IR and Raman Spectra, Neutron Diffraction of Fe(OH)₂. *Journal of Molecular Structure* **1994**, *328*, 121–132. [https://doi.org/10.1016/0022-2860\(94\)08355-X](https://doi.org/10.1016/0022-2860(94)08355-X).
- (27) Gui, W.-B.; Zhao, C.-S.; Liu, J. Phase Stability and Hydroxyl Vibration of Brucite Mg(OH)₂ at High Pressure and High Temperature. *Chinese Phys. Lett.* **2021**, *38* (3), 038101. <https://doi.org/10.1088/0256-307X/38/3/038101>.
- (28) Tian, H.; Li, Y.; Zhang, J.; Ma, Y.; Wang, Y.; Wang, Y.; Li, Y.; Cui, Q. High Pressure Induced Phase Transformation through Continuous Topology Evolution in Zinc Hydroxyfluoride Synthesized via a Hydrothermal Strategy. *Journal of Alloys and Compounds* **2017**, *726*, 132–138. <https://doi.org/10.1016/j.jallcom.2017.07.317>.